

**PCCP****Abnormal Linear Elasticity in Polycrystalline Phosphorene**

Journal:	<i>Physical Chemistry Chemical Physics</i>
Manuscript ID	CP-ART-12-2017-008540.R1
Article Type:	Paper
Date Submitted by the Author:	28-Feb-2018
Complete List of Authors:	Liu, Ning; University of Georgia, College of Engineering Pidaparti, Ramana; University of Georgia, College of Engineering Wang, Xianqiao; University of Georgia, College of Engineering

SCHOLARONE™  
Manuscripts

## Abnormal Linear Elasticity in Polycrystalline Phosphorene

Ning Liu, Ramana Pidaparti and Xianqiao Wang\*

College of Engineering, University of Georgia, Athens, GA 30602 USA

\*Corresponding author: [xqwang@uga.edu](mailto:xqwang@uga.edu)

### Abstract

Phosphorene, also known as monolayer black phosphorous, has been widely used in electronic devices due to its superior electrical properties. However, its relatively low Young's modulus, low fracture strength and susceptibility to structural failure has limited its application in nano devices. Therefore, in order to design more mechanically reliable devices that utilize phosphorene, it is necessary to explore the mechanical properties of polycrystalline phosphorene. Here molecular dynamics simulations are performed to study the effect of grain size on the mechanical performance of polycrystalline phosphorene sheets. Unlike other two-dimension materials with planar crystalline structure, polycrystalline phosphorene sheets are almost linear elastic, resulting from its high bending stiffness due to its intrinsic buckled crystalline structure. Moreover, the percentage increase of stiffness for polycrystalline phosphorene associated with the increase of grain size from 2 to 12 nm is only 15.9%, much smaller than that for other two-dimension materials with planar crystalline structure. This insensitivity could be attributed to the small difference between the elastic modulus of the crystalline phase and amorphous phase of polycrystalline phosphorene. In addition, the strength deduction obeys well a logarithm relation of grain size, well explained by the dislocation pile-up theory analogous to that of polycrystalline graphene. Overall, our findings provide a better understanding of mechanical properties of polycrystalline phosphorene and establish a guideline for manufacturing and designing novel phosphorene-based nano devices and nano structures.

**Keywords:** polycrystalline phosphorene, strength reduction, grain size, annealing process, molecular dynamics

## 1. Introduction

In recent years, extensive efforts have been made to synthesize 2D materials with exceptional electrical, optical, thermal, and mechanical properties, such as graphene,<sup>1</sup> hexagonal boron nitride,<sup>2</sup> silicene,<sup>3</sup> molybdenum disulfide,<sup>4</sup> borophene,<sup>5</sup> and phosphorene.<sup>6</sup> Phosphorene, a counterpart of bulk black phosphorus, has been mechanically exfoliated in the form of a few layers<sup>7</sup> or even a single layer<sup>8</sup>. Due to its unique physical properties, such as a finite and direct band gap<sup>9</sup> and high free carrier mobility<sup>10</sup>, phosphorene has been explored as a new two-dimensional material for applications in nanoelectronics devices. Despite exceptional electrical properties, phosphorene has relatively low Young's modulus, low fracture strength, and susceptibility to structural failure, limiting its application in nano devices. Therefore, in order to design more mechanically reliable devices that utilize phosphorene, it is necessary to explore the mechanical properties of phosphorene structures.

Recent years have witnessed a growth of interest in the understanding of mechanical properties of single crystalline phosphorene sheets via both computational and experimental investigations. For example, using first principle calculations, Jiang *et al.* reported the existence of a negative Poisson's ratio in a single layer phosphorene.<sup>11</sup> Unlike engineered bulk auxetics, this intrinsic property of phosphorene originates from its uniquely puckered structure. Wang *et al.* studied the mechanical properties of a single layer phosphorene and found that the Young's modulus of phosphorene is one order of magnitude smaller than that of graphene, opening a new window for promising applications based on large-magnitude-strain engineering.<sup>12</sup> Kou *et al.* unveiled a highly anisotropic ripple pattern in phosphorene.<sup>13</sup> Results indicate that the compression-induced ripple deformation occurs only along the zigzag direction in the range up to 10% strain, but not in armchair direction. This orientation-selective ripple deformation patterns originates from its puckered structure with a coupled hinge-like bonding configuration and an anisotropic Poisson ratio. Zhang *et al.* studied the mechanical properties of phosphorene under different temperature using molecular dynamics simulations.<sup>14</sup> The predicted strength and moduli are in good agreement with available experimental and first principle calculation results. Liu *et al.* studied the fracture pattern and energy release rate of phosphorene using molecular dynamics simulations.<sup>15</sup> Their results indicate that fracture under uniaxial tension along the armchair direction is attributed to the break in the interlayer bond angles, while failure in the zigzag direction is triggered by the break in both intra-layer angles and bonds. With respect to the energy release rate, when the crack orientation changes, the variation in the armchair direction is small while the fluctuation in the zigzag direction is very large. From these previous studies, we know that unlike graphene with highly symmetric hexagonal crystalline structure, pristine phosphorene sheets have highly anisotropic mechanical properties. However, most current studies focus on the single crystalline

phosphorene in terms of mechanical properties, the mechanical properties of polycrystalline phosphorene remains largely unexplored.

Large size 2D materials are likely to exist in a polycrystalline form such as graphene.<sup>16</sup> There should be no exception for polycrystalline phosphorene although it has not been reported yet. The existence of polycrystalline phosphorene can be foreseen if the chemical vapor deposition method is used for synthesization like the observation in graphene.<sup>16</sup> Polycrystalline 2D materials, with unavoidable line defects also known as grain boundaries, behave differently compared with their pristine counterparts in terms of physical properties, especially mechanical properties.<sup>17-25</sup> Song *et al.* performed a series of molecular dynamics simulations to study the fracture of polycrystalline graphene, which indicates that as the grain size decreases, fracture strength increases.<sup>25</sup> The above phenomenon can be well explained by a dislocation pileup model. Moreover, the role of grain boundary ends and junctions is emphasized, which is ignored by previous studies. Unlike graphene, individual phosphorene sheets are highly anisotropic with respect to mechanical properties. For example, Young's moduli of phosphorene in the armchair and zigzag direction are 38.4 and 145.9 GPa respectively while the ultimate strength for armchair and zigzag are approximately 10 and 25 GPa respectively,<sup>26</sup> much lower than that of pristine graphene (130 GPa).<sup>27</sup> In addition to high anisotropy, the configuration of phosphorene is inherently puckered in the thickness direction. All these unique properties may deeply influence the mechanical properties of polycrystalline phosphorene with similar architecture as polycrystalline graphene. Therefore, there is a critical need for the investigation of the mechanical properties of polycrystalline phosphorene.

Here we perform molecular dynamics simulations to understand the effect of grain size on the mechanical properties of polycrystalline phosphorene. The average grain size of polycrystalline sheets ranges from 2 to 12 nm while the number of grains are fixed at 64. The effect of number of grains on corresponding results is presented in Figure S1 and discussed in the supplemental material. For each given grain size, polycrystalline phosphorene sheets are generated through Voronoi tessellation, prepared through the annealing process and thus mechanically tested through biaxial tension in order to obtain mechanical properties, such as ultimate strength and in-plane elastic modulus, *etc.* The detailed procedure and the effect of annealing process on the mechanical properties can be found in Figure S2, S3 and S4 in the supplemental material. It turns out that polycrystalline phosphorene exhibits unusual linear elasticity compared with other two-dimension materials and the in-plane elastic modulus is abnormally insensitive to the variance of grain size. We conclude our paper with an in depth discussion on the fundamental mechanisms of grain-size dependent mechanical properties.

## 2. Methods

Figure 1(a) shows the geometrical model of polycrystalline is generated through Voronoi decomposition<sup>28</sup>. The total number of grains is fixed at 64 while the average size of the grains ranges from 2 to 12nm. The number of grains play a marginal role in the mechanical properties of polycrystalline phosphorene. Corresponding results are presented in Figure S1 in the supplemental material. In order to exclude the shape effect of individual grains, the Voronoi tessellation plan is fixed as shown in Figure 1(a) while the grain orientation for each individual grain are varied to get five independent samples for each specific grain size. It is worth noting that the size of the sample is in scale with grain size. The crystalline structure of phosphorene is shown in Figure 1(b). Unlike graphene, phosphorene has in-plane puckered structure. Corresponding geometrical parameters can be found in our previous studies<sup>15,29</sup>.

A reactive force field (ReaxFF)<sup>26</sup> for phosphorus/hydrogen system is adopted to describe the interactions among atoms inside the phosphorene sheets. Compared with the nonreactive Stillinger-Webber potential<sup>30</sup>, the ReaxFF used here has shown greater reliability and robustness in describing the mechanical properties of both pristine and defected phosphorene<sup>26</sup>. ReaxFF is a bond-order potential force field. Unlike conventional empirical force field, ReaxFF requires no predefined connectivity claims, such as explicit bonds, angles and dihedrals. Instead, ReaxFF allows automatic breaking and forming of bonds during the simulation. In the current ReaxFF, the bond stretching energy ( $E_{bond}$ ) are corrected with an overcoordination penalty energy ( $E_{over}$ ). In addition, energy contributions from valence angle ( $E_{val}$ ) and torsion angle ( $E_{tors}$ ) are also included. Dispersion interactions are described by the combination of the original van der Waals (vdW) term ( $E_{vdw}$ ) and low-gradient vdW correction term ( $E_{lgvdw}$ )<sup>31</sup>. Energy contributions from electrostatic interactions ( $E_{Coulomb}$ ) are taken into account between all atom pairs, where the atomic charges are calculated based on connectivity and geometry using the electron equilibration method (EEM)<sup>32</sup>. The total potential energy for the phosphorene system is expressed as follows,

$$E_{total} = E_{bond} + E_{over} + E_{val} + E_{tors} + E_{vdw} + E_{lgvdw} + E_{Coulomb} \quad (1)$$

The detailed expressions of each term<sup>33</sup> and relevant parameters<sup>26</sup> can be found in previous works.

All the simulations are performed based on the package LAMMPS<sup>34</sup> developed by Sandia National Laboratory. Unless otherwise stated, the time step is fixed at 1.0 femtosecond. In order to obtain physically stable model configurations, phosphorene samples with certain grain sizes generated through Voronoi tessellation algorithm are annealed before tensile tests. The annealing process can be briefly described as follows. First, energy minimization is carried out to avoid atom-overlapping in grain boundaries. Subsequently, the sample temperature is continuously increased from 1 K to 800K in 50 picoseconds, controlled at 800K for another 100 picoseconds, and finally decreased to 1K in 50 picoseconds under the NVT ensemble. After the annealing process, the annealed samples are further relaxed to mitigate the huge

internal residual stress through alternating between NVT and NPT ensemble with  $T=1\text{K}$ . Finally, these pretreated polycrystalline phosphorene sheets are biaxially stretched for investigating their mechanical properties. During the biaxial tensile test, the NVT ensemble is adopted with  $T=1\text{K}$  and periodic boundary conditions are used in the in-plane directions of the sheets. The polycrystalline sheets are stretched stepwise with strain rate  $0.02\% \text{ ps}^{-1}$  by extending the box size on both in-plane directions simultaneously and then relaxed for a period of 5 ps until the next addition of strain. To eliminate thermal noise, an average biaxial stress is obtained from the data in the last 500 time steps of the relaxation stage for a certain strain and adopted as the output stress for the following analysis. All simulation results are also visualized by the package Open Visualization Tool (OVITO)<sup>35</sup>.

### 3. Results and Discussions

Due to the prestress on the grain boundaries, polycrystalline 2D materials have large out-of-plane distortions compared with their pristine counterparts even at very low temperature<sup>18, 25, 36</sup>. Because of the huge differences between in-plane and out-of-plane stiffness, polycrystalline silicene and graphene show a strong strain-hardening effect upon stretching as the out-of-plane distortion is flattened out. However, with comparable in-plane and out-of-plane stiffness, polycrystalline phosphorene can avoid the influence of out-of-plane distortion on stress-strain responses, showing an almost constant stiffness under stretching. According to the previous researches, the out-of-plane stiffness for graphene<sup>37</sup> is around 1.2 eV while the counterparts for phosphorene<sup>38</sup> are 4.3 and 8.6 eV on armchair and zigzag direction, respectively. On the other hand, the in-plane elastic modulus for pristine graphene<sup>27</sup> is around 1000 GPa while those for pristine phosphorene are 38.4 and 145.9 GPa on armchair and zigzag direction, respectively. In order to validate the above hypothesis, 5 samples with different grain orientation profiles but identical grain morphologies shown in Figure 1 are prepared for both polycrystalline phosphorene and graphene using annealing process. The average grain is fixed at 2 nm. The out-of-plane distortion of polycrystalline graphene samples are  $15.8\pm 2.4 \text{ \AA}$  while the out-of-plane distortion for phosphorene is  $13.6\pm 1.7 \text{ \AA}$ . When we normalize these quantities by dividing them by their out-of-plane thickness (3.5 and 5.2  $\text{\AA}$  for graphene and phosphorene, respectively), the difference is even larger ( $4.5\pm 0.7$  and  $2.6\pm 0.3$  for graphene and phosphorene, respectively). These huge differences could lead to significantly different mechanical behaviors between phosphorene and graphene at the very beginning of the deformation. As expected, the stress-strain response for polycrystalline graphene is rather nonlinear while that for polycrystalline phosphorene is almost linear as shown in Figure 2(a). To clarify the origin of this significant difference, the out-of-plane height profiles for both phosphorene and graphene sheets during the deformation are shown in Figure 2(b), in which only the profiles before strain 0.03 are shown for concision. As we can see from the first column of Figure 2(b), there are a lot of atoms colored with red and blue for graphene, meaning that the out-of-plane height is high

for those atoms and thus the initial configuration is rather wavy. However, as the strain increases, blue and red regions shrink, indicating that the sheets are flattening. As a result, the slope of the stress-strain curve for graphene in Figure 2(a), representing the in-plane stiffness, increases. After the graphene sheet is almost flattened, the stress-strain curve of the graphene sheet becomes linear, meaning that the stiffness does not change anymore. In contrast to graphene, there are few regions with red and blue color for phosphorene sheet before tension as we can see from Figure 2(b), meaning that the initial configuration is rather flat. This flat configuration leads to a pretty straight stress-strain curve for phosphorene sheet until failure. These findings validate our previous hypothesis that due to the comparable in-plane and out-of-plane stiffness, the mechanical behavior of polycrystalline phosphorene is abnormally linear elastic.

To further confirm the abnormal linear elasticity of polycrystalline phosphorene, samples with different grain sizes were prepared and mechanically tested in the same manner. Figure 3 shows average stress-strain responses of polycrystalline phosphorene sheets with different grain size ( $d$ ) under biaxial tensile tests. As we can see, polycrystalline phosphorene sheets still behave like typical linear elastic materials. Moreover, as  $d$  increases, the slope of the curves, representing the in-plane elastic modulus ( $S$ ), increases. Figure 4(a) shows  $S$  versus  $d$ , indicating that  $S$  ranges from  $62.5 \pm 1.8$  GPa to  $72.8 \text{ GPa} \pm 0.8$  GPa with the increase of grain size from  $d = 2$  to 12 nm. These results are the stiffness in the armchair (38.4 GPa) and zigzag (145.9 GPa) direction of pristine phosphorene sheets<sup>26</sup>, which should be reasonable. In addition to simulation results, there is also a fitting curve shown in Figure 4(a), indicating that  $S$  is linearly related to the inverse of grain size, in which the detailed formula is  $S = 73.3 - 24.0d^{-1}$ . However, compared with other polycrystalline materials, polycrystalline phosphorene is less sensitive to  $d$  in terms of  $S$ . For example, the stiffness of polycrystalline graphene increases from 650 GPa to 950 GPa with the same increase range of grain size<sup>18</sup>. Polycrystalline silicene experiences a 42.8 percent stiffness enhancement, from 35 N/m to 50 N/m, with the same increase range of grain size<sup>36</sup>. Polycrystalline boron nitride shows an intensive improvement regarding stiffness, from 120 GPa to 200 GPa, with the increase of grain size from 3 to 12 nm<sup>17</sup>. Other relevant results are summarized in Table 1, showing that elastic modulus of polycrystalline phosphorene  $S$  is least sensitive to grain size  $d$ .

The stiffness presented in Figure 4 (a) were in fact the slope of stress-strain curves in Figure 3. In Figure 3, the stress plotted is the average of axial stress on two axes which are shown in Figure 1. In other words, the plotted stress can be expressed as  $\frac{\sigma_{xx} + \sigma_{yy}}{2}$ . Moreover, the biaxial tensile tests were carried out through applying identical strain simultaneously on both x and y axes. Therefore, for each grain of the polycrystalline sheet, the stress-strain relation can be expressed as follows,

$$\begin{pmatrix} \sigma_{11} \\ \sigma_{22} \\ \sigma_{12} \end{pmatrix} = \begin{pmatrix} C_{1111} & C_{1122} & C_{1112} \\ C_{2211} & C_{2222} & C_{2212} \\ C_{1211} & C_{1222} & C_{1212} \end{pmatrix} \begin{pmatrix} \varepsilon \\ \varepsilon \\ 0 \end{pmatrix} \quad (2)$$

where the subscript “1” represents x axis while “2” represents y axis. The plotted stress can then be expressed as  $\sigma = \frac{\sigma_{11} + \sigma_{22}}{2} = \frac{C_{1111} + C_{1122} + C_{2211} + C_{2222}}{2} \varepsilon$ . Therefore, the nominal stiffness for each grain in the biaxial tensile test is  $S_g = \frac{C_{1111} + C_{1122} + C_{2211} + C_{2222}}{2}$ . Note that, if in tensor form, it can be expressed as  $S_g = \frac{C_{ijjj}}{2}$ ,  $i, j = 1, 2$ . The quantity  $C_{ijjj}$  is an invariant of the given tensor, which means that even after coordinate transformation this quantity still does not change. Thus, regardless of different orientations, the stiffness  $S_g$  remains constant for every grain inside the sheet. To verify this statement we have performed biaxial tensile tests on single crystalline phosphorene with different orientations from  $15^\circ$  to  $75^\circ$ . The results are presented in Figure S5 and relevant discussions are also available in the supplemental materials. Therefore, the overall stiffness  $S$  should be identical to  $S_g$ . However, due to the weakening role of grain boundaries in stiffness, the overall stiffness  $S$  should be smaller than  $S_g$ . As it is shown in Figure 4(a),  $S$  increases with the inverse of grain size  $d$ . In fact, the percentage of grain boundary phase also increase with the inverse of grain size  $d$  as shown in Figure 5 (a). Grain boundary atoms are defined as atoms with atomic von Mises stress greater than 5 GPa. As it is shown in the inset Figure 5 (a), the atoms between two or among three adjacent grains are usually with high von Mises stress. Those atoms are also loosely connected by covalent bonds compared with those atoms inside the grain, among which there are a lot of defects such as dangling bonds. Therefore, this so-called amorphous grain boundary phase is softer than that of crystalline phase of phosphorene, weakening the stiffness  $S$  of polycrystalline phosphorene. However, as the grain size  $d$  increases, the percentage of grain boundary phase decreases and approaches zero, leading to the increase of stiffness  $S$  to the idealized stiffness of crystalline phase  $S_g$ . The above mechanism is also applicable for other polycrystalline 2D materials. However, there is something unexpected in phosphorene shown in Figure 5(b). As the grain size increases from 1 to 12nm, the percentage of amorphous grain boundary phase decreases from 84.3% to 14.8%, which is even obvious and straightforward when comparing the snapshots in the inset of Figure 5(a). On the other hand, the stiffness  $S$  only increases by 41.9%, from 51.3 to 72.8 GPa, which indicate that the difference between stiffness of amorphous grain boundary phase and that of crystalline phase is marginal. In a word, due to the marginal difference between stiffness of grain boundary phase and crystalline phase of phosphorene, the stiffness  $S$  of polycrystalline phosphorene is insensitive to grain size  $d$ .

Figure 4(b) shows the results of ultimate strength ( $\sigma_u$ ) versus grain size  $d$ , indicating a strength reduction from  $5.42 \pm 0.36$  GPa to  $4.11 \pm 0.29$  GPa associated with the increase of grain size from  $d = 2$  to 12 nm. The simulation results also fit to a linear form of logarithm function and the estimated relationship is  $\sigma_u = 6 - 0.75 \ln(d)$ . As it is discussed in the previous studies, the weakening effect of finite grain boundaries could be quantitatively interpreted using the continuum elastic theory of dislocations<sup>25</sup>. The stress calculations for a semi-infinite grain boundary of graphene shows that as the length of grain boundary increases the prestress at the end of grain boundary increases and fits the linear form of logarithm function<sup>25</sup>. Similarly, the junctions in polycrystalline materials, where more than two grains interact with each other, should be severe stress-concentration sites and the amplitude of stress-concentration should follow the same rule as the ends of semi-infinite grain boundaries. Therefore, as the grain size increases, the prestress in the junctions increases, accelerating the initiation of fracture and thus reducing the ultimate strength under stretching, which is so-called dislocation pileup theory<sup>25</sup>. To further validate the above strength reduction law, the snapshots of polycrystalline phosphorene sheets in Figure 6 show the crack initiation and subsequent propagation for a polycrystalline sheet with grain size  $d = 12$  nm. Figure 6 (a) shows the crack initiation site while Figure 6(b) gives a more detailed view, indicating that the crack initiation indeed starts at the junction. After initiation, cracks branches into three different paths: two of them go inside grains while the other one propagate along the grain boundary.

#### 4. Conclusions

In summary, molecular dynamics simulations are adopted to systematically study the effect of grain size on mechanical properties of polycrystalline phosphorene. Results indicate that unlike other two-dimension materials with planar crystalline structure, stress-strain responses of polycrystalline phosphorene are almost linear at the beginning of deformation, instead of strain-hardening. This unusual linear elasticity is recognized in polycrystalline phosphorene with grain sizes ranging from 2 to 12 nm and could be attributed to the small out-of-plane distortion of unloaded polycrystalline phosphorene, induced by its high bending stiffness due to its intrinsic buckled crystalline structure. In addition to its unusual linear elasticity, polycrystalline phosphorene is also less sensitive to grain size  $d$  with respect to in-plane elastic modulus  $S$ . The percentage increase of  $S$  for polycrystalline phosphorene associated with the increase of grain size from 2 to 12 nm is only 15.9%, much smaller than that for other materials with planar crystalline structure, such as graphene, silicene and hexagonal boron-nitride. This insensitivity could be attributed to the small difference between the elastic modulus of the crystalline phase and amorphous phase of polycrystalline phosphorene. The dependence of ultimate strength  $\sigma_u$  on grain size  $d$  is captured by a linear form of logarithm function. The above logarithm relation can be well explained by the dislocation pile-up theory, which is further confirmed by the crack nucleation sites upon stretching. Overall, our findings provide a

better understanding of mechanical properties of polycrystalline phosphorene and establish a guideline for manufacturing and designing novel phosphorene-based nano devices and nano structures.

### **Acknowledgement**

N.L., X.W, and R.P. acknowledge the support from the National Science Foundation (Grant No. CMMI-1610812). Computational simulations are performed at the UGA Advanced Computing Resource Center.

## Figures

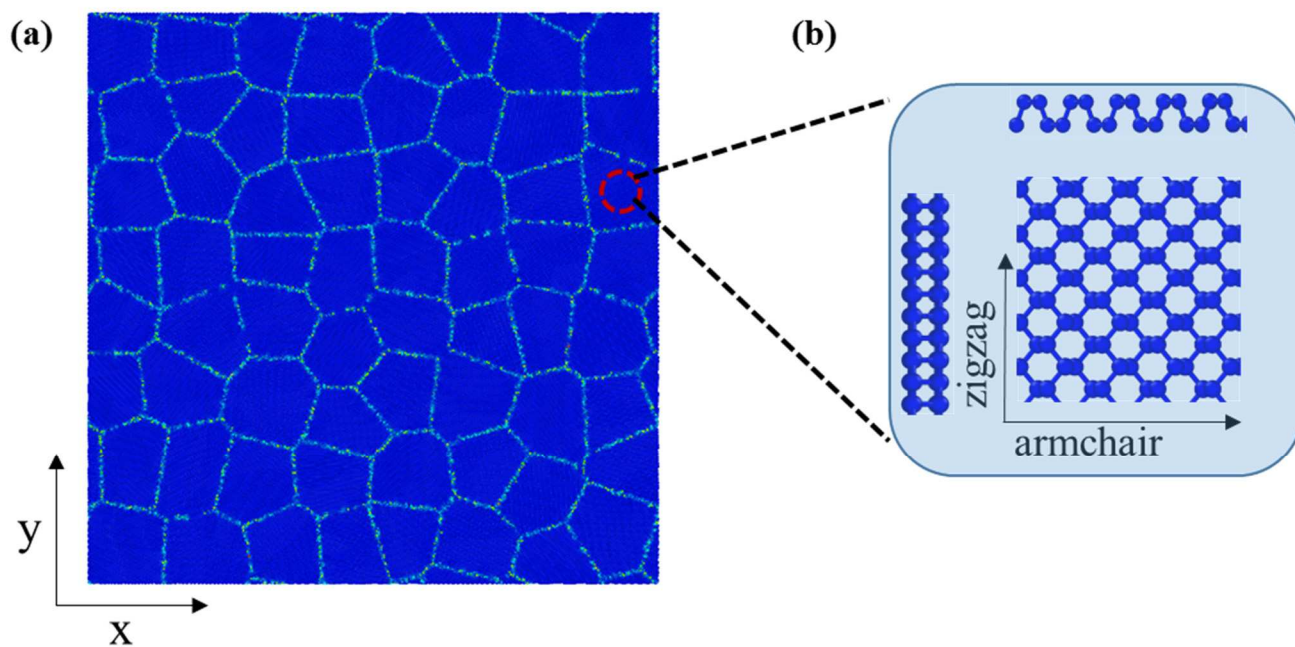


**Figure 1.** (a) Top view of a polycrystalline phosphorene sheet from the Voronoi tessellation method; (b) A zoomed-in snapshot inside a single grain with detailed atomic crystalline structure.

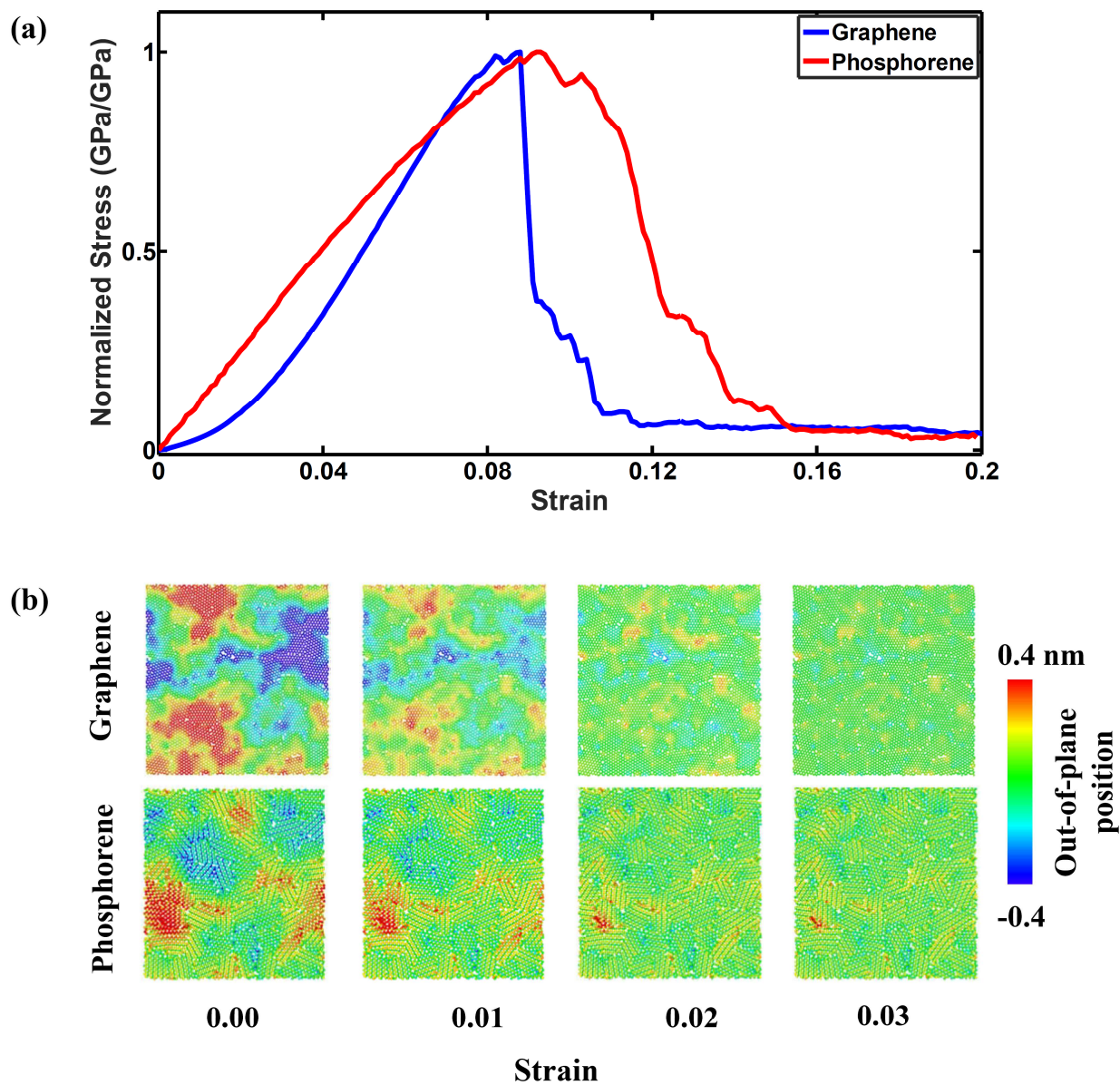


**Figure 2.** (a) Normalized stress-strain responses of polycrystalline graphene and phosphorene sheets under biaxial tension. (b) Profile of out-of-plane height of atoms during the tension test. (The average grain size is 2nm)

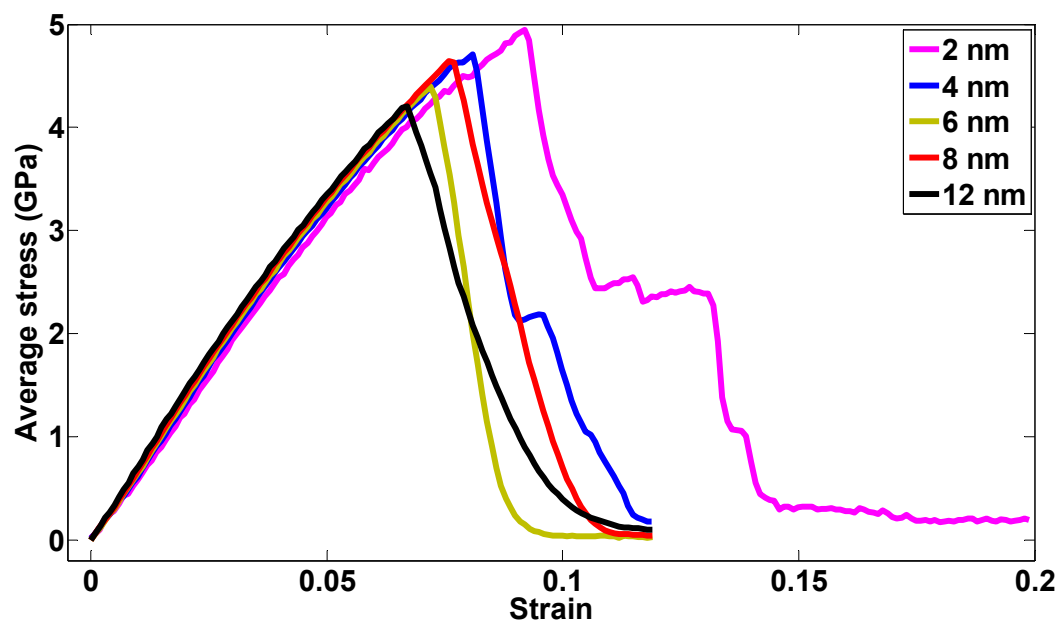


**Figure 3.** Average stress-strain responses under a biaxial tensile test for polycrystalline phosphorene sheets with varying grain sizes.

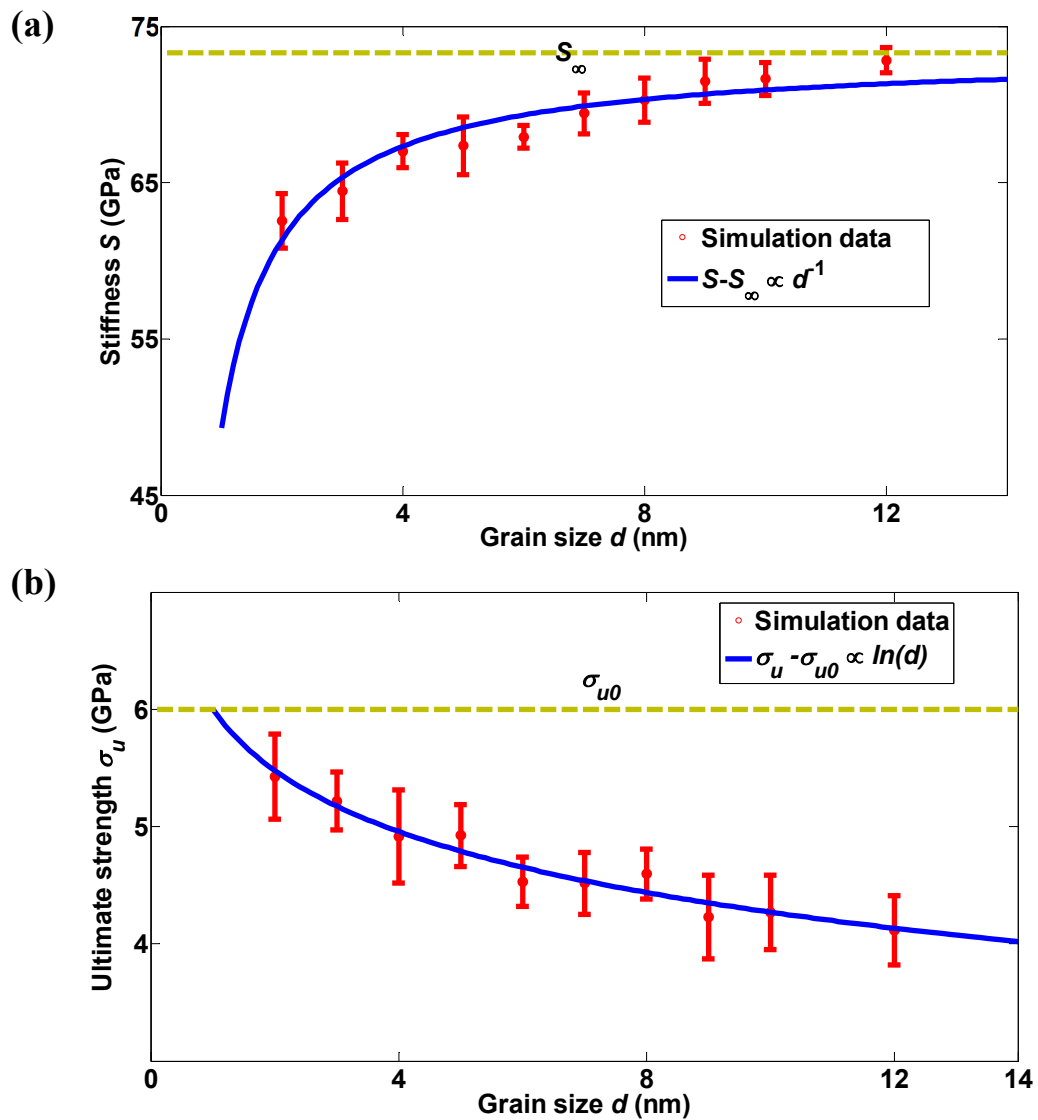


**Figure 4.** Mechanical properties versus grain size for polycrystalline phosphorene sheets (a) Stiffness  $S$  (b) Ultimate strength  $\sigma_u$ .

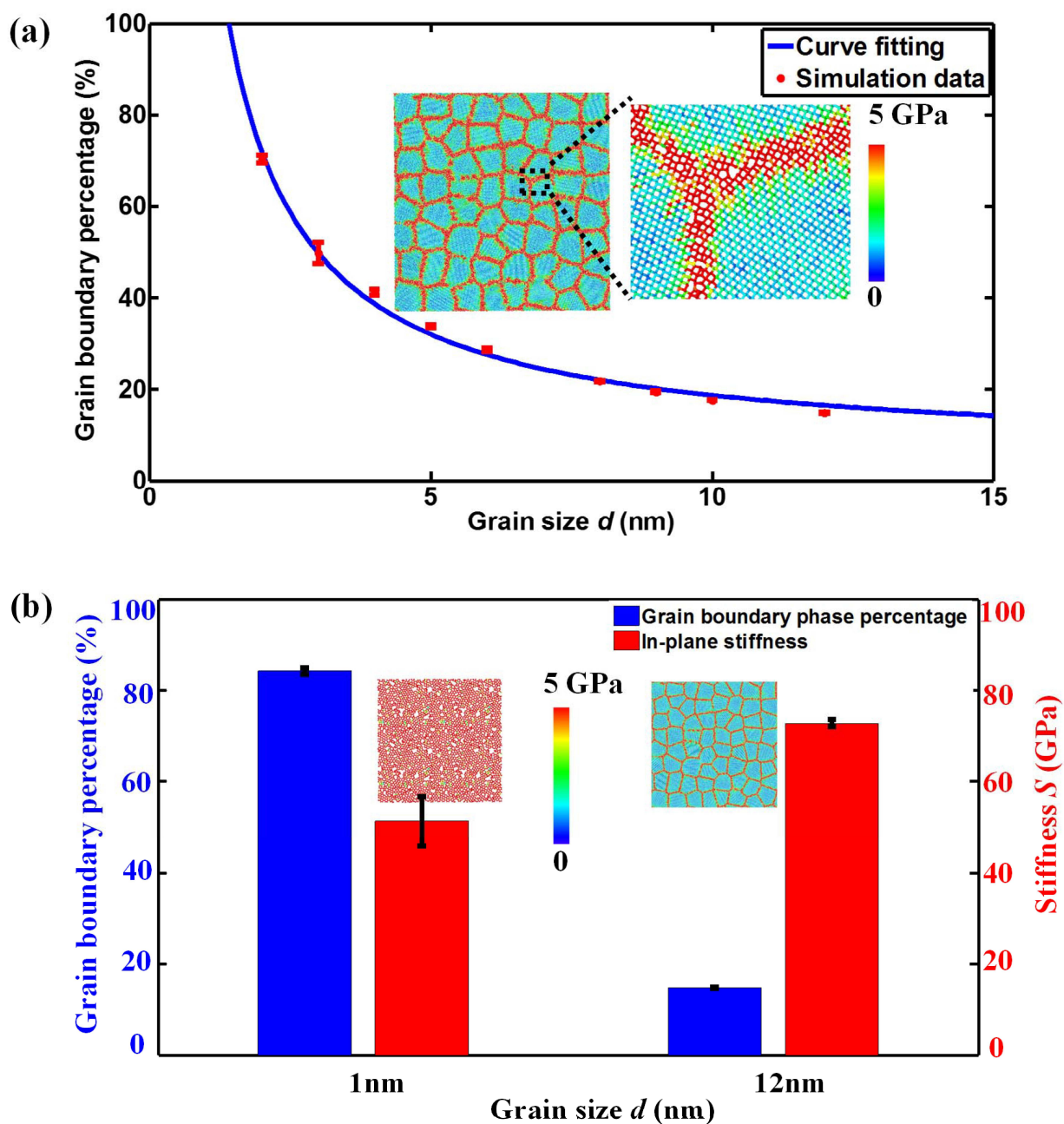


**Figure 5** (a) Grain boundary percentage versus grain size (b) Comparison of stiffness between amorphous phase and crystalline phase of polycrystalline phosphorene (The insets are colored by von Mises stress.)

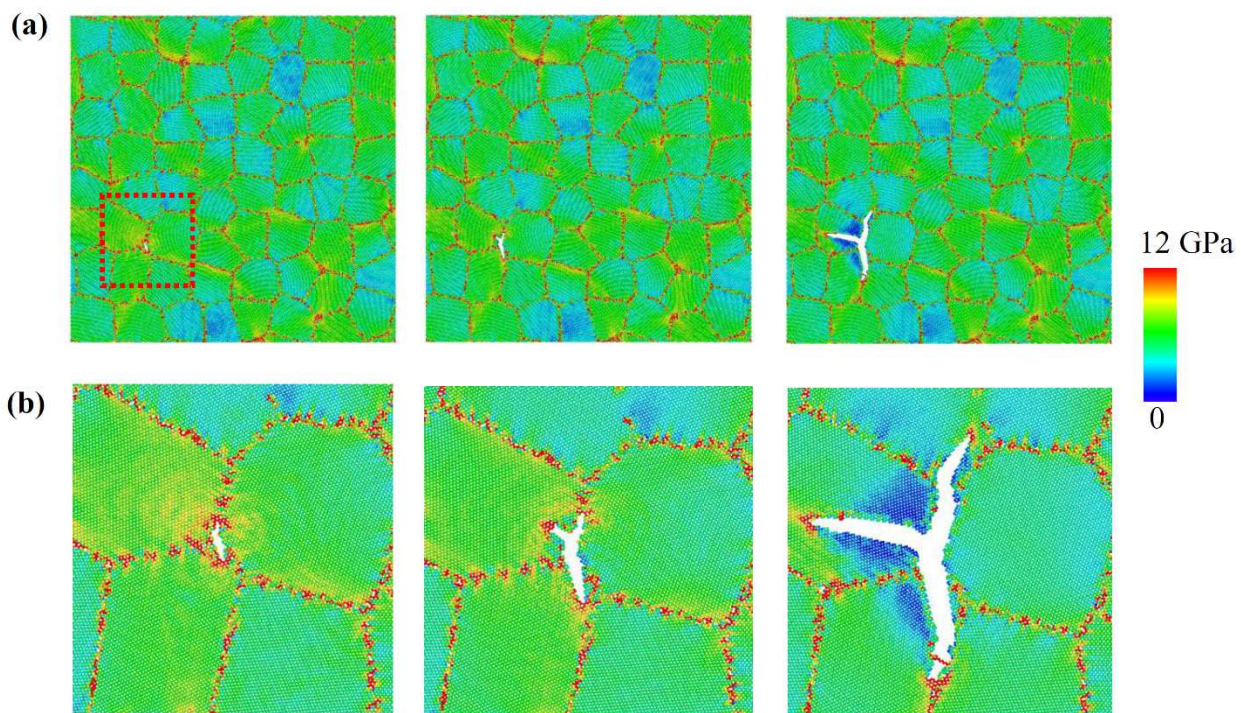


**Figure 6.** (a) The global crack propagation process of a polycrystalline phosphorene sheet with 12 nm grain size  $d = 12$  nm when the strain  $\epsilon$  is around 6.9%; (b) Zoomed-in snapshot of a critical area highlighted by red dash square in the subfigure (a) (All the snapshots are colored by atomic von Mises stress)

## Tables

Table 1. In-plane stiffness/elastic modulus of different polycrystalline 2D materials

Type of 2D materials	Grain size range (nm)	Variance of in-plane stiffness/elastic modulus
Graphene <sup>39</sup>	2 to 12	650 to 950 GPa (46.1% increase)
Graphene <sup>40</sup>	3 to 11	625 to 850 GPa (34.6% increase)
Graphene <sup>25</sup>	2 to 5	675 to 900 GPa (33.3% increase)
Silicene <sup>23</sup>	2 to 12	35 to 50 N/m (42.8% increase)
Hexagonal boron-nitride <sup>41</sup>	2 to 10	490 to 720 GPa (46.9% increase)
Hexagonal boron-nitride <sup>17</sup>	3 to 12	120 to 200 GPa (66.6% increase)
Phosphorene (Current work)	2 to 12	63 to 73 GPa (15.9% increase)

## References

1. K. S. Novoselov, A. K. Geim, S. V. Morozov, D. Jiang, Y. Zhang, S. V. Dubonos, I. V. Grigorieva and A. A. Firsov, *Science*, 2004, **306**, 666-669.
2. K. Watanabe, T. Taniguchi and H. Kanda, *Nature Materials*, 2004, **3**, 404-409.
3. B. Aufray, A. Kara, S. Vizzini, H. Oughaddou, C. Leandri, B. Ealet and G. Le Lay, *Applied Physics Letters*, 2010, **96**, 3.
4. K. F. Mak, C. Lee, J. Hone, J. Shan and T. F. Heinz, *Physical Review Letters*, 2010, **105**, 4.
5. A. J. Mannix, X. F. Zhou, B. Kiraly, J. D. Wood, D. Alducin, B. D. Myers, X. L. Liu, B. L. Fisher, U. Santiago, J. R. Guest, M. J. Yacaman, A. Ponce, A. R. Oganov, M. C. Hersam and N. P. Guisinger, *Science*, 2015, **350**, 1513-1516.
6. H. Liu, A. T. Neal, Z. Zhu, Z. Luo, X. Xu, D. Tománek and P. D. Ye, *ACS Nano*, 2014, **8**, 4033-4041.
7. L. Li, Y. Yu, G. J. Ye, Q. Ge, X. Ou, H. Wu, D. Feng, X. H. Chen and Y. Zhang, *Nat Nano*, 2014, **9**, 372-377.
8. H. Liu, A. T. Neal, Z. Zhu, Z. Luo, X. F. Xu, D. Tomanek and P. D. D. Ye, *ACS Nano*, 2014, **8**, 4033-4041.
9. X. H. Peng, Q. Wei and A. Copple, *Phys. Rev. B*, 2014, **90**, 10.
10. B. L. Liao, J. W. Zhou, B. Qiu, M. S. Dresselhaus and G. Chen, *Phys. Rev. B*, 2015, **91**, 8.
11. J.-W. Jiang and H. S. Park, *Nat Commun*, 2014, **5**.
12. Q. Wei and X. Peng, *Applied Physics Letters*, 2014, **104**, 251915.
13. L. Kou, Y. Ma, S. C. Smith and C. Chen, *The Journal of Physical Chemistry Letters*, 2015, **6**, 1509-1513.
14. Z. Y. Yang, J. H. Zhao and N. Wei, *Applied Physics Letters*, 2015, **107**, 5.
15. N. Liu, J. Hong, R. Pidaparti and X. Wang, *Nanoscale*, 2016, **8**, 5728-5736.
16. A. Reina, X. T. Jia, J. Ho, D. Nezich, H. B. Son, V. Bulovic, M. S. Dresselhaus and J. Kong, *Nano Letters*, 2009, **9**, 30-35.
17. M. Becton and X. Wang, *Physical Chemistry Chemical Physics*, 2015, **17**, 21894-21901.
18. M. Becton, X. Zeng and X. Wang, *Carbon*, 2015, **86**, 338-349.
19. M. Bohayra and C. Gianaurelio, *Nanotechnology*, 2014, **25**, 215704.
20. S. Goverapet Srinivasan and A. C. T. van Duin, *The Journal of Physical Chemistry A*, 2011, **115**, 13269-13280.
21. Y. Guo, C. Qiao, A. Wang, J. Zhang, S. Wang, W.-S. Su and Y. Jia, *Physical Chemistry Chemical Physics*, 2016, **18**, 20562-20570.
22. N.-N. Li, Z.-D. Sha, Q.-X. Pei and Y.-W. Zhang, *The Journal of Physical Chemistry C*, 2014, **118**, 13769-13774.
23. L. Ning, H. Jiawang, P. Ramana and W. Xianqiao, *2D Mater.*, 2016, **3**, 035008.
24. C. Pinqiang, W. Jianyang, Z. Zhisen and N. Fulong, *Nanotechnology*, 2017, **28**, 045702.
25. Z. Song, V. I. Artyukhov, B. I. Yakobson and Z. Xu, *Nano Letters*, 2013, **13**, 1829-1833.
26. H. Xiao, X. Shi, F. Hao, X. Liao, Y. Zhang and X. Chen, *The Journal of Physical Chemistry A*, 2017, **121**, 6135-6149.
27. C. Lee, X. Wei, J. W. Kysar and J. Hone, *Science*, 2008, **321**, 385-388.
28. F. Aurenhammer, *Computing Surveys*, 1991, **23**, 345-405.
29. N. Liu, J. Hong, X. Zeng, R. Pidaparti and X. Wang, *Physical Chemistry Chemical Physics*, 2017, **19**, 13083-13092.
30. J. W. Jiang, *Nanotechnology*, 2015, **26**, 8.
31. L. Liu, Y. Liu, S. V. Zybin, H. Sun and W. A. Goddard, *The Journal of Physical Chemistry A*, 2011, **115**, 11016-11022.

32. G. O. A. Janssens, B. G. Baekelandt, H. Toufar, W. J. Mortier and R. A. Schoonheydt, *The Journal of Physical Chemistry*, 1995, **99**, 3251-3258.
33. A. C. T. van Duin, S. Dasgupta, F. Lorant and W. A. Goddard, *The Journal of Physical Chemistry A*, 2001, **105**, 9396-9409.
34. S. Plimpton, *Journal of Computational Physics*, 1995, **117**, 1-19.
35. A. Stukowski, *Model. Simul. Mater. Sci. Eng.*, 2010, **18**, 7.
36. N. Liu, J. W. Hong, R. Pidaparti and X. Q. Wang, *2D Mater.*, 2016, **3**, 10.
37. M. K. Bles, A. W. Barnard, P. A. Rose, S. P. Roberts, K. L. McGill, P. Y. Huang, A. R. Ruyack, J. W. Kevek, B. Kobrin, D. A. Muller and P. L. McEuen, *Nature*, 2015, **524**, 204.
38. Z. Hao-Yu and J. Jin-Wu, *Journal of Physics D: Applied Physics*, 2015, **48**, 455305.
39. M. Becton, X. Zeng and X. Wang, *Carbon*, 2015, **86**, 338-349.
40. Z. D. Sha, S. S. Quek, Q. X. Pei, Z. S. Liu, T. J. Wang, V. B. Shenoy and Y. W. Zhang, *Scientific Reports*, 2014, **4**, 5991.
41. B. Mortazavi and G. Cuniberti, *RSC Advances*, 2014, **4**, 19137-19143.